JACS
JOURNAL OF THE AMERICAN CHEMICAL SOCIETY
Article
pubs.acs.org/JACS

Zigzag Sc_2C_2 Carbide Cluster inside a [88]Fullerene Cage with One Heptagon, $Sc_2C_2@C_s(hept)$-C_{88}: A Kinetically Trapped Fullerene Formed by C_2 Insertion?

Chia-Hsiang Chen,[†,⊥,∥] Laura Abella,[§,⊥] Maira R. Cerón,[†,#] Miguel A. Guerrero-Ayala,[†] Antonio Rodríguez-Fortea,[§] Marilyn M. Olmstead,[*,‡] Xian B. Powers,[‡] Alan L. Balch,[*,‡] Josep M. Poblet,[*,§] and Luis Echegoyen[*,†]

[†]Department of Chemistry, University of Texas at El Paso, El Paso, Texas 79968, United States
[‡]Department of Chemistry, University of California at Davis, One Shields Avenue, Davis, California 95616, United States
[§]Departament de Química Física i Inorgànica, Universitat Rovira i Virgili, C/Marcel·lí Domingo 1, 43007 Tarragona, Spain

Supporting Information

ABSTRACT: A non-isolated pentagon rule metallic carbide clusterfullerene containing a heptagonal ring, $Sc_2C_2@C_s(hept)$-C_{88}, was isolated from the raw soot obtained by electric arc vaporization of graphite rods packed with Sc_2O_3 and graphite powder under a helium atmosphere. The $Sc_2C_2@C_s(hept)$-C_{88} was purified by multistage high-performance liquid chromatography (HPLC), cocrystallized with Ni−(octaethylporphyrin), and characterized by single-crystal X-ray diffraction. The diffraction data revealed a zigzag Sc_2C_2 unit inside an unprecedented $C_s(hept)$-C_{88} carbon cage containing 13 pentagons, 32 hexagons, and 1 heptagon. Calculations suggest that the observed nonclassical fullerene could be a kinetically trapped species derived from the recently reported $Sc_2C_2@C_{2v}(9)$-C_{86} via a direct C_2 insertion.

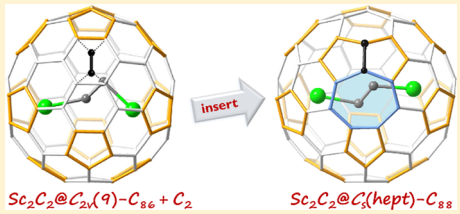

INTRODUCTION

Fullerenes are a general class of compounds composed of closed carbon cages possessing 12 five-membered rings and a variable number of six-membered rings. Unfunctionalized empty fullerenes always have pentagons surrounded by five hexagons, thus obeying the isolated pentagon rule (IPR).[1] Closed fullerene structures containing fused pentagons (pentalene units) are strongly destabilized because of local steric strain caused by enforced bond angles accompanied by higher pyramidalization of the carbon atoms.[2,3] However, some fullerenes are not only composed of pentagons and hexagons but also contain other polygons, such as heptagons.[4] The heptagon-containing fullerenes are usually less stable compared with IPR empty fullerenes because heptagon formation is always accompanied by the presence of pentalene units, in violation of the IPR.[5] Exohedral halogenation can stabilize non-IPR fullerenes, making heptagon-containing fullerenes possible, by transforming sp^2- to sp^3-carbon hybridization, thus releasing some of the strain of the fused pentagons.[5−10] Endohedral metal clusters can also stabilize pentalene structures, but to the best of our knowledge, only one endohedral fullerene, $LaSc_2N@C_s(hept)$-C_{80}, has been reported, which contains a heptagonal ring.[11]

One of the most fascinating properties of fullerenes is their ability to encapsulate atoms, ions, small molecules or metallic clusters.[12,13] Endohedral metallofullerenes (EMFs) exhibit a variety of electronic and physicochemical properties that markedly depend on the nature of the encapsulated species.[14−18] In 2001, Shinohara and co-workers unambiguously assigned the structure of Sc_2C_{86} as the first metal carbide clusterfullerene, $Sc_2C_2@D_{2d}(23)$-C_{84}, as opposed to $Sc_2@C_{86}$.[19] The observation that M_2C_2 units can be trapped inside fullerene cages means that M_2C_{2n} endohedral fullerenes can exist either as $M_2@C_{2n}$ compounds or as carbides, $M_2C_2@C_{2n-2}$. The crystallographically characterized metal carbide clusterfullerenes include the following: $Sc_2C_2@C_s(10528)$-C_{72},[12] $Sc_2C_2@C_{2v}(5)$-C_{80},[20,21] $Sc_2C_2@C_{3v}(8)$-C_{82},[21−23] $Sc_2C_2@D_{2d}(23)$-C_{84},[19] $Gd_2C_2@C_1(51383)$-C_{84},[24] $Gd_2C_2@D_3(85)$-C_{92},[25] $Tm_2C_2@C_s(6)$-C_{82},[26] $Tb_2C_2@C_s(6)$-C_{82},[27] $Sc_2C_2@C_{2v}(9)$-C_{86},[28] $La_2C_2@D_5(450)$-C_{100},[29] $La_2C_2@C_s(574)$-C_{102}, and $La_2C_2@C_2(816)$-C_{104}.[30] Interestingly, in most of the reported cases, the M_2C_2 cluster exhibits what has been described as a folded butterfly shape with considerable disorder, particularly in the positions of the metal centers with respect to the C_2 unit.[2,12] However, a few exceptions have been reported. $Sc_2C_2@C_{2v}(9)$-C_{86} has a planar unsymmetrical but ordered Sc_2C_2 unit, while $La_2C_2@C_s(574)$-C_{102}, $La_2C_2@C_2(816)$-C_{104}, and $La_2C_2@D_5(450)$-C_{100} show considerable disorder but have an irregular zigzag configuration for the La_2C_2 cluster.

Dorn and co-workers reported that the size of a fullerene cage could influence the shape of the inner M_2C_2 cluster in endohedral fullerenes.[31] They suggested that decreasing the size of the fullerene would compress M_2C_2 clusters from a

Received: July 30, 2016
Published: September 5, 2016

DOI: 10.1021/jacs.6b07912
J. Am. Chem. Soc. 2016, 138, 13030−13037

nearly linear, stretched geometry to a constrained butterfly structure. Deng and Popov also suggested that M_2C_2 units can adopt different orientations with respect to the metal atoms depending on the shape of the host carbon cage.[32] We recently reported the structure of $Sc_2C_2@C_{2v}(9)$-C_{86}, where the Sc_2C_2 cluster exhibits a planar shape between a butterfly and a distorted linear geometry. It is interesting to know what specific shape the Sc_2C_2 will adopt inside a higher fullerene cage. Here, we report a zigzag Sc_2C_2 unit inside an unprecedented C_s(hept)-C_{88} carbon cage, $Sc_2C_2@C_s$(hept)-C_{88}, the first example of an endohedral carbide fullerene with a heptagon ring. In addition, calculations show that this is not the thermodynamically favored structure, so we suggest that it is a kinetically favored compound obtained by a simple C_2 addition directly on the recently reported $Sc_2C_2@C_{2v}(9)$-C_{86} cage, an interesting and important mechanistic possibility.

RESULTS AND DISCUSSION

Preparation and Purification of $Sc_2C_2@C_s$(hept)-C_{88}. Carbon soot containing empty cage fullerenes and scandium endohedral fullerenes was obtained by vaporizing a graphite rod filled with Sc_2O_3 and graphite powder (molar ratio of Sc/C = 1:15) in a modified Krätschmer–Huffman arc-discharge reactor under a 200 mbar helium atmosphere. The soot was collected and extracted with refluxing carbon disulfide for 12 h. Upon solvent removal, the resulting mixture of empty fullerenes and scandium containing endohedral fullerenes was analyzed by HPLC using a 5PYE column with toluene as the mobile phase and a flow rate of 3.00 mL min^{-1}, as shown in Figure S1a. Four isomers of Sc_2C_{90} were found, but only Sc_2C_{90}(I) was obtained in a reasonable yield and was relatively easy to isolate. The Sc_2C_{90}(I) fraction coelutes with Sc_2C_{90}(II), Sc_2C_{90}(III), $Sc_2C_2@C_{2v}(9)$-C_{86}, and C_{94} (fraction A). Sc_2C_{90}(IV) was found in fraction B. Fraction A was further separated by three additional HPLC stages (details are described in the Supporting Information) and resulted in the isolation of pure Sc_2C_{90}(I) (see Figure S1).

The matrix-assisted laser desorption/ionization-time of flight mass spectrometry (MALDI-TOF MS) spectrum (Figure 1) of the isolated fraction shows a single peak at m/z 1169.905. The isotopic distribution of the experimental MALDI-TOF spectrum nicely matches the calculated spectrum for Sc_2C_{90}(I). The purity of this sample was further confirmed by HPLC as shown in Figure S1.

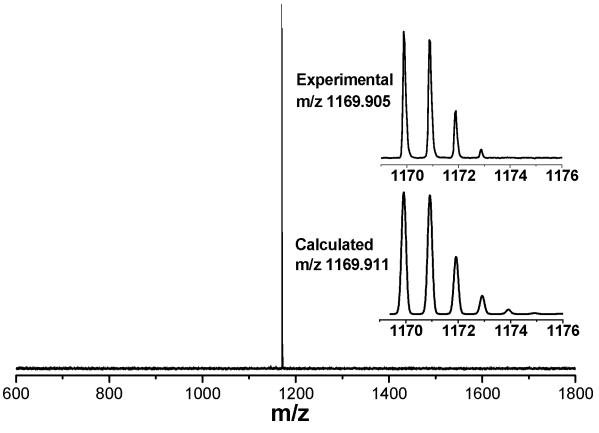

Figure 1. Mass spectrum of the purified Sc_2C_{90}(I). Inset: experimental and calculated isotopic distributions for Sc_2C_{90}(I).

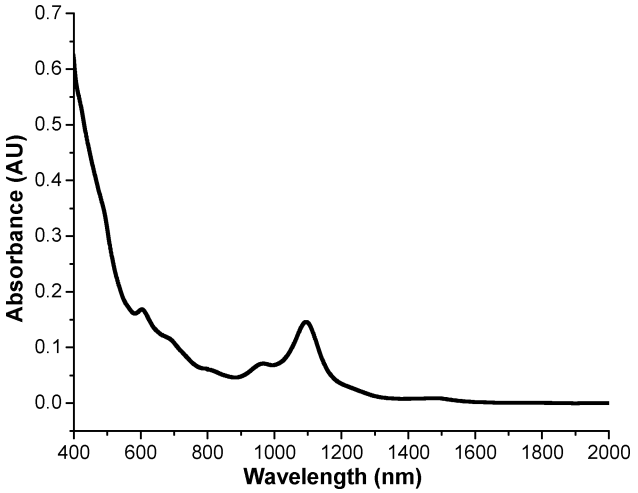

Figure 2. Vis–NIR absorption of Sc_2C_{90}(I) in CS_2 solution.

Spectroscopic and Electrochemical Characterization of $Sc_2C_2@C_s$(hept)-C_{88}. Figure 2 shows the vis–NIR absorption spectrum of a CS_2 solution of Sc_2C_{90}(I). A strong absorption was observed at 1094 nm with other absorptions at 491, 603, 696, 808, 966, and 1478 nm. As previously discussed, Sc_2C_{90}(I) can exist as either a dimetallic endohedral fullerene, $Sc_2@C_{90}$, or as a carbide, $Sc_2C_2@C_{88}$. Vis–NIR absorption spectra typically are fingerprint signatures of the specific fullerene cages and their electronic structures[33] because the electronic absorption spectra of endohedral fullerenes in the visible and NIR are mostly due to π–π^* transitions of the fullerene cages.[34] The characteristic features of the observed spectrum are substantially different from those reported for endohedral fullerenes possessing C_{90} cages such as Sm@$C_2(40)$-C_{90},[35] Sm@$C_2(42)$-C_{90},[35] Sm@$C_2(45)$-C_{90},[35] Sm@$C_2(46)$-C_{90},[35] and $Sm_2@C_1(21)$-C_{90},[36] which have been crystallographically characterized. The vis–NIR spectrum is also substantially different from those of the crystallographically characterized $Sm_2@D_2(35)$-C_{88}[36] and $Tb_3N@D_2(35)$-C_{88}.[37] The remarkable differences between the absorption spectrum of Sc_2C_{90}(I) and those of all of the reported C_{88} and C_{90} isomeric cages are consistent with the presence of a totally different carbon cage symmetry.

The electrochemical properties of $Sc_2C_2@C_s$(hept)-C_{88} were measured by cyclic voltammetry (CV) using a glassy carbon minielectrode with *o*-dichlorobenzene and tetra(*n*-butyl)-ammonium hexafluorophosphate (*o*-DCB/*n*-Bu_4NPF_6) as solvent/electrolyte (Figure S2). The CV results, summarized in Table 1, show four reversible and one irreversible reductive processes likely centered on the carbon cage along with one reversible oxidation. Compared to the other reported endohedral fullerene containing a heptagon ring, $LaSc_2N@I_h$-C_{80},[11] we observe very different redox processes. The reduction potentials are anodically shifted and the oxidation potential is cathodically shifted. As a result, we observed a decrease in the

Table 1. Redox Potentials (V) vs Fc/Fc^+ Couple of $Sc_2C_2@C_s$(hept)-C_{88}

$Sc_2C_2@C_{88}$	$\varepsilon^{0/+}$	$\varepsilon^{0/-}$	$\varepsilon^{-/2-}$	$\varepsilon^{2-/3-}$	$\varepsilon^{3-/4-}$	$\varepsilon^{4-/5-}$
ε_{pc}	0.32	−0.84	−1.76	−2.05	−2.31	−2.54
ε_{pa}	0.43	−0.73		−1.95	−2.19	−2.42

DOI: 10.1021/jacs.6b07912
J. Am. Chem. Soc. 2016, 138, 13030–13037

electrochemical band gap in agreement with the low abundance of $Sc_2C_2@C_s(hept)$-C_{88}.

Crystallographic Identification of $Sc_2C_2@C_s(hept)$-C_{88}. Figure 3 shows the structure of the endohedral fullerene as

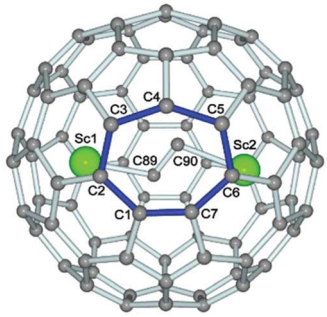

Figure 3. A view of the structure of $Sc_2C_2@C_s(hept)$-C_{88}. Only one of the two orientations of the cage is shown.

determined from single-crystal X-ray diffraction of the black cocrystal $Sc_2C_2@C_s(hept)$-C_{88}·Ni(OEP)·2(C_7H_8). The crystallographic results reveal that the molecule contains an Sc_2C_2 unit inside a carbon cage with one heptagon, outlined in blue in Figure 3, 13 pentagons, rather than the usual 12, and 32 hexagons. The carbon cage has C_s idealized symmetry. There is only one abutting pair of pentagons, which is adjacent to the heptagon. The structure suffers from some disorder. The asymmetric unit contains one endohedral fullerene, which is disordered into two equally occupied orientations, an ordered Ni(OEP) molecule, and two disordered molecules of toluene.

As illustrated in Figure 4, the Sc_2C_2 unit has a planar, zigzag structure, rather than the more common, folded butterfly arrangement found in other carbide-containing endohedral fullerenes. The Sc_2C_2 unit is disordered but in a fashion that is clearly connected to the cage disorder. Figure 4 shows the geometry of the Sc_2C_2 unit inside each of the two cage orientations. Sc1 is common to both orientations, while one orientation involves Sc2A with the other orientation utilizing Sc2B. The average C−C distance of the carbide is 1.215(7) Å. The carbide is twisted such that the Sc−C distances differ (see Figure 4). The two nonbonded Sc---Sc distances are 4.825(2) Å and 4.812(2) Å. The disorder in this carbide structure is notably less than that found in most other carbide-containing endohedrals with the exception of $Sc_2C_2@C_{2v}(9)$-C_{86}, which has no disorder in the position of the Sc_2C_2 unit.[28] In Figure 4, the shape of the Sc_2C_2 unit in $Sc_2C_2@C_s(hept)$-C_{88} is also compared to the corresponding unit in $Sc_2C_2@C_{2v}(9)$-C_{86}.[28] In $Sc_2C_2@C_{2v}(9)$-C_{86}, the Sc_2C_2 unit is also planar but twisted into an irregular shape that places C87 in an unusual, asymmetric position between Sc1 and Sc2. Overall, the comparison of the structures reveals that enlargement of the fullerene cage is accompanied by stretching of the Sc_2C_2 unit in accord with the predictions of Dorn and co-workers and Deng and Popov.[31,32] Carbide clusters of the type M_2C_2 with a butterfly shape generally show considerable disorder in the metal positions, probably because there is cylindrical symmetry in the π-orbitals of the carbide unit. The planar M_2C_2 units in $Sc_2C_2@C_s(hept)$-C_{88} and $Sc_2C_2@C_{2v}(9)$-C_{86} also utilize Sc(III) with a high charge density that helps to orient the carbide units. The two scandium ions are situated near the centers of hexagons on the inside of the carbon cage. They have typical distances to interior cage carbons, although Sc1 has some

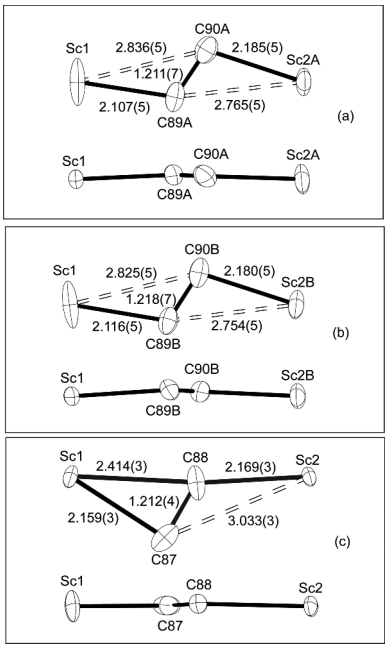

Figure 4. Carbide geometry for cage A (a) and cage B (b) of $Sc_2C_2@C_s$-(hept)-C_{88} and for $Sc_2C_2@C_{2v}(9)$-C_{86} (c). Thermal displacement parameters are depicted at the 35% probability level. In each box, the top view is down the least-squares plane of the four atoms and the bottom view is rotated by 90° toward the viewer, showing the planarity of the unit. Torsion angles are 175.3(2)°, 173.1(2)°, and 177.0(2)°, and the Sc---Sc distances span 4.825(2) Å, 4.812(2) Å, and 4.5760(6) Å for (a), (b), and (c), respectively.

shorter Sc−C contacts and is positioned less centrally to its hexagonal ring. These distances as well as the C−C distances in the heptagonal ring are given in Table S1.

Computational Analysis of $Sc_2C_2@C_s(hept)$-C_{88} and Other Sc_2C_{90} Isomers. To assess the stability of the crystallographic structure and to propose likely cages for the other three detected Sc_2C_{90} isomers, DFT computations were done (see Computational Details). Besides the $Sc_2C_2@C_{88}$ carbide clusterfullerenes (CCFs), classical dimetallic endohedral fullerenes of the type $Sc_2@C_{90}$ were also considered. For the C_{88} cage, there are 81738 possible isomers, but only 35 of them follow the IPR. Given the formal transfer of four electrons from Sc_2C_2 to the C_{88} cage, described as $(Sc_2C_2)^{4+}@(C_{88})^{4-}$, we have computed the tetraanions for all of the C_{88} IPR cages (35) and non-IPR isomers with up to two adjacent pentagon pairs (APP): 368 APP1 and 2304 APP2. The lowest energy tetraanionic cages, within a range of 23 kcal·mol^{-1}, were selected, and the corresponding $Sc_2C_2@C_{88}$ structures were optimized (see the Computational Details). On the other hand, there are 99918 isomers for the C_{90} cage, and only 46 of them satisfy the IPR. In this case, the electronic structures of the $Sc_2@C_{90}$ metallofullerenes result from a formal transfer of six electrons from the metal atoms to the cage, $(Sc_2)^{6+}@(C_{90})^{6-}$. Thus, we have computed the energies of the hexaanions for all cages with two or less adjacent pentagon pairs: 46 IPR, 544 APP1, and 3454 APP2 isomers. The lowest hexaanionic cages (less than 10 kcal·mol^{-1}) were chosen and optimized as $Sc_2@C_{90}$ metallofullerenes. The IPR isomers $D_2(35)$-C_{88} and $C_2(43)$-C_{90} were found to be the lowest energy C_{88}^{4-} and C_{90}^{6-} anions, respectively (see Table 2). It should be noted that the crystallographically characterized $Sm_2@D_2(35)$-C_{88} with an internal $(Sm_2)^{4+}$ unit utilizes the $D_2(35)$-C_{88} cage.[36] Although

DOI: 10.1021/jacs.6b07912
J. Am. Chem. Soc. 2016, 138, 13030−13037

Table 2. Relative Energies and HOMO−LUMO (H−L) Gaps for the Selected Isomers of C_{88} and C_{90} in the Corresponding Anionic and Endohedral Forms[a,b]

isomer	C_{90}^{6-}	$Sc_2@C_{90}$	H−L gap
$Sc_2@C_2(44)$-C_{90}	4.3	0.0	0.773
$Sc_2@C_2(42)$-C_{90}	9.2	4.5	0.567
$Sc_2@C_2(43)$-C_{90}	0.0	5.0	0.548
$Sc_2@C_1(21)$-C_{90}	9.9	9.9	0.410
isomer	C_{88}^{4-}	$Sc_2C_2@C_{88}$	H−L gap
$Sc_2C_2@D_2(35)$-C_{88}	0.0	2.1	0.751
$Sc_2C_2@C_s(32)$-C_{88}	8.5	3.6	0.709
$Sc_2C_2@C_1(26)$-C_{88}	7.2	8.7	0.810
$Sc_2C_2@C_s$(hept)-$C_{88}(2)$[b]	15.0	10.4	0.738
$Sc_2C_2@C_1(78749)$-C_{88}	19.0	12.2	0.683
$Sc_2C_2@C_1(74790)$-C_{88}	19.4	12.7	0.731
$Sc_2C_2@C_1(70333)$-C_{88}	23.0	13.1	0.531
$Sc_2C_2@C_s$(hept)-$C_{88}(1)$[b]	15.0	18.8	0.625

[a]Energies in kcal·mol^{-1}, H−L gaps in eV. [b]Same isomer, but a different cluster orientation is shown in parentheses for $Sc_2C_2@C_s$(hept)-C_{88}.

the lowest energy EMF corresponds to the IPR dimetallic $Sc_2@C_2(44)$-C_{90}, the next most stable isomers are the CCFs $Sc_2C_2@D_2(35)$-C_{88} at only 2.1 kcal·mol^{-1} and $Sc_2C_2@C_s(32)$-C_{88} at 3.6 kcal·mol^{-1}. The X-ray characterized structure, $Sc_2C_2@C_s$(hept)-C_{88} (1), once optimized, was found to be at 18.8 kcal·mol^{-1}. The optimized Sc−C distances are 2.17 Å for Sc1−C89, 3.37 Å for Sc1−C90, 2.69 Å for Sc2−C89, and 2.10 Å for Sc2−C90, in rather good agreement with the X-ray data (see Table S1). Interestingly, a second minimum in which the Sc_2C_2 cluster is perpendicular with respect to the orientation found in the X-ray structure, $Sc_2C_2@C_s$(hept)-C_{88}(2), is found at a lower energy (10.4 kcal·mol^{-1}, see Table 2 and Figure 5).

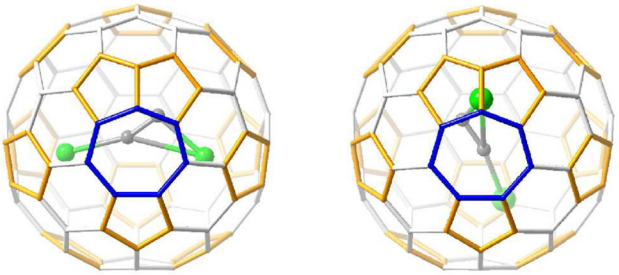

Figure 5. Optimized structures of $Sc_2C_2@C_s$(hept)-C_{88} with two different orientations of the internal dimetallic carbide. Orientation 1 is the one found in the X-ray structure; orientation 2, with the cluster rotated around 90 degrees, is 8.4 kcal mol^{-1} lower in energy than 1. Pentagons are highlighted in orange, and the heptagon is in blue.

The molar fractions of the lowest energy $Sc_2C_2@C_{88}$ and $Sc_2@C_{90}$ isomers as a function of the temperature were also computed using the rigid rotor and harmonic oscillator (RRHO) approximation and the related free-encapsulated model (FEM) as proposed by Slanina (see Figure 6 and SI).[38,39] For $Sc_2C_2@C_s$(hept)-C_{88}, we have considered the X-ray structure, $Sc_2C_2@C_s$(hept)-C_{88}(1).

Both approximations predict $Sc_2C_2@D_2(35)$-C_{88} as the most abundant isomer for temperatures lower than 1000 K. Another IPR carbide clusterfullerene, $Sc_2C_2@C_s(32)$-C_{88}, was found to be the second most abundant isomer up to 1000 K and the most abundant one at higher temperatures (T > 1000 K). The abundance of the X-ray characterized structure, $Sc_2C_2@C_s$(hept)-C_{88}(1), increases slightly at high temperatures but remains less than 10% at temperatures of fullerene formation (2000−3000 K). Although the X-ray structure does not correspond to the theoretically computed most stable orientation of the Sc_2C_2 unit at the present level of calculation, both orientations are practically degenerate at high temperatures (the free energy difference at 2000 K is only 3 kcal mol^{-1}; see the SI for more details). The molar fractions of classical dimetallofullerenes are negligible in the whole range of temperatures. According to these results, isomers $Sc_2C_2@C_s(32)$-C_{88} and $Sc_2C_2@D_2(35)$-C_{88} are likely to be among the other three isomers of Sc_2C_{90} found experimentally but not isolated. We confirmed that the relative stabilities of $Sc_2C_2@C_s$(hept)-C_{88}, $Sc_2C_2@D_2(35)$-C_{88}, and $Sc_2C_2@C_s(32)$-C_{88} isomers do not depend on the computational settings. Other density functionals (PBE, B3LYP, and M06) or the introduction of dispersion corrections results in similar predictions for their relative stabilities (see Table S4).

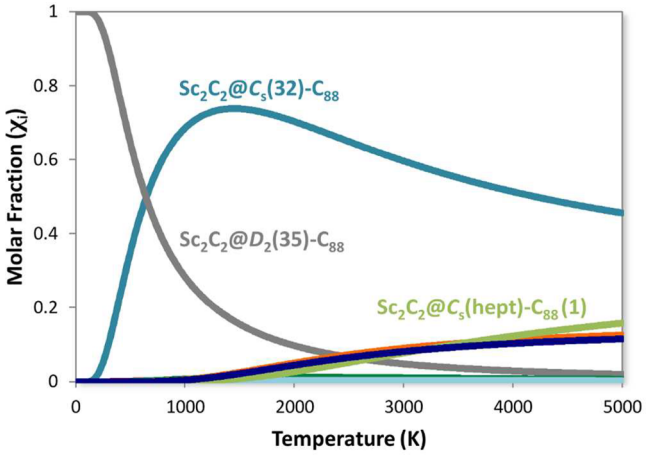

Figure 6. Predicted molar fractions within the RRHO approximation as a function of temperature for the selected $Sc_2@C_{90}$ and $Sc_2C_2@C_{88}$ isomers (see the SI for a detailed description).

The frontier molecular orbitals of $Sc_2C_2@C_s$(hept)-C_{88} confirm that there is a formal transfer of four electrons from the Sc_2C_2 unit to the C_{88} cage, i.e., $(Sc_2C_2)^{4+}@(C_{88})^{4-}$ (see the SI). The HOMO and the LUMO are mainly localized on the cage. We have analyzed the electrochemical properties for some possible Sc_2C_{90} candidates (see Table S5). The results for $Sc_2C_2@C_s$(hept)-C_{88} are in agreement with the experimental data. The first oxidation and reduction potentials are computed (experimental value in parentheses) to be 0.34 V (0.38 V) and −0.70 V (−0.78 V), respectively. The predicted EC gap is 1.03 V, which compares well with the experimental value (1.16 V). The computed UV−vis−NIR spectrum using time-dependent (TD) DFT for the $Sc_2C_2@C_s$(hept)-C_{88} isomer shows transitions at 622, 770, 903, 1183, and 1302 nm (see SI).

Car−Parrinello molecular dynamics simulations (see the SI for more details) of $Sc_2C_2@C_s$(hept)-C_{88}(1) at room temperature and at temperatures of fullerene formation (2000 K) were also performed to gain more insight about the motion of the Sc_2C_2 cluster inside the C_s(hept)-C_{88} fullerene. We have seen that the Sc_2C_2 unit essentially keeps the original orientation for trajectories that last 30 ps at room temperature (see Figure 7). The average of the Sc−C distances in the Sc_2C_2 unit reasonably matches the value found by X-ray crystallography (see Table

DOI: 10.1021/jacs.6b07912
J. Am. Chem. Soc. 2016, 138, 13030−13037

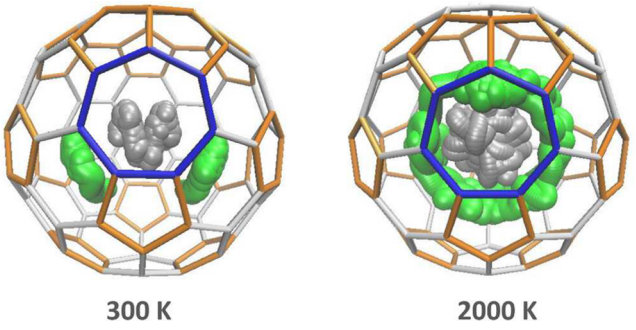

Figure 7. Motion of the Sc_2C_2 cluster inside the C_s(hept)-C_{88} cage along the Car−Parrinello simulation at 300 K (30 ps) and 2000 K (20 ps). Pentagons are highlighted in orange, and heptagon is in blue.

S2). However, at 2000 K, the mobility of the scandium carbide in the cage is much higher, which led to the observation of another stable orientation of the cluster inside the cage, the above-mentioned $Sc_2C_2@C_s$(hept)-C_{88}(2). The cluster changes the initial orientation to finally get the optimal one in only 3.6 ps. The much higher mobility of the cluster at high temperatures is evident in Figure 7.

How Is $Sc_2C_2@C_s$(hept)-C_{88} Formed? A Kinetically Trapped EMF Consistent with a Bottom-up Growth Mechanism. At this point, we wondered about the formation of this unique nonclassical heptagon-containing EMF, which might provide valuable insight about the formation mechanism of endohedral fullerenes. Recently, Echegoyen, Balch, and co-workers synthesized, isolated, and characterized the carbide clusterfullerene $Sc_2C_2@C_{2v}(9)$-C_{86}. Interestingly, a direct relationship between the X-ray characterized structures of $Sc_2C_2@C_{2v}(9)$-C_{86} and $Sc_2C_2@C_s$(hept)-C_{88} has been found. Isomer $Sc_2C_2@C_s$(hept)-C_{88} could have been formed by a simple C_2 insertion on $Sc_2C_2@C_{2v}(9)$-C_{86} (see Figure 8). When

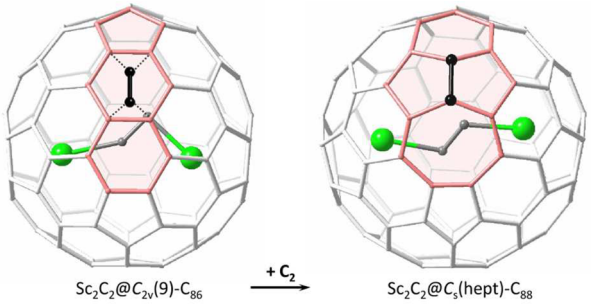

Figure 8. Structural relationship between $Sc_2C_2@C_{2v}(9)$-C_{86} and $Sc_2C_2@C_s$(hept)-C_{88} by a C_2 insertion. The motif that is involved in the transformation is highlighted in pink. The inserted C_2 unit is highlighted in black.

a C_2 unit is added at the selected hexagon, one hexagon, one heptagon, and two fused pentagons are formed in the new structure (see Figure 8). The process is highly favorable at 0, 300, and 2000 K. $Sc_2C_2@C_{2v}(9)$-C_{86} is found to be the lowest energy (thermodynamic) isomer of the $Sc_2C_2@C_{86}$ family, followed by $Sc_2C_2@C_{2v}(15)$-C_{86} at 4.7 kcal·mol^{-1} (see Table S7). We have confirmed that the orientation of the Sc_2C_2 cluster inside the $C_{2v}(9)$-C_{86} cage is (i) the one with the lowest energy among all those other orientations analyzed and (ii) the most frequent one in a 40 ps Car−Parrinello MD trajectory at 2000 K (see the SI). In addition, the computed molar fractions (both RRHO and FEM approximations) predict the lowest energy isomer $Sc_2C_2@C_{2v}(9)$-C_{86} to be the most abundant in the complete temperature range, i.e. the thermodynamic isomer, with $Sc_2C_2@C_{2v}(15)$-C_{86} as the second most abundant isomer (see Figure S11).

To shed light on the formation mechanism of $Sc_2C_2@C_s$(hept)-C_{88}, we analyzed all of the possible single C_2 insertions to the tetraanionic cages $C_{2v}(9)$-C_{86} and $C_{2v}(15)$-C_{86} that led to classical and nonclassical heptagon-containing C_{88} fullerenes. Figure 9 shows the two types of additions

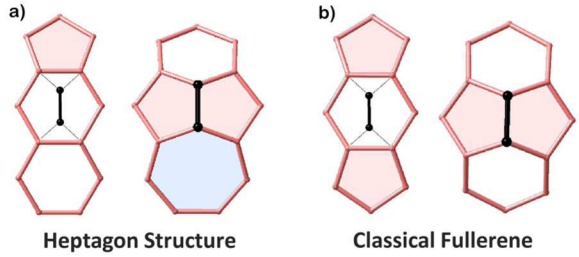

Figure 9. C_2 insertion on a hexagon forming (a) a heptagon-containing cage or (b) a classical fullerene. Pentagons are colored in pink, hexagons in white, and heptagon in blue.

analyzed. We found that cage C_s(hept)-C_{88}, the one found by X-ray crystallography to contain the Sc_2C_2 cluster, is the lowest energy cage among all the different possibilities. Two classical APP1 cages and a heptagon-containing cage are at 7, 8, and 11 kcal mol^{-1}, respectively; the other cages are found at 20 and 80 kcal mol^{-1} (see Figure S16). Once the heptagon-containing EMF is formed, why is it detected and isolated? The likely answer to this query is that this nonclassical cage cannot evolve easily to a more stable classical IPR or non-IPR cage. At least *four bond* rearrangements are required to obtain some APP1 and APP2 isomers, such as $C_1(70333)$-C_{88}, $C_1(78749)$-C_{88}, $C_1(81690)$-C_{88}, $C_1(66771)$-C_{88}, $C_1(66889)$-C_{88}, and $C_1(66708)$-C_{88}. A minimum of five rearrangements are needed to transform the cage structure of C_s(hept)-C_{88} into the IPR $D_2(35)$-C_{88} cage. It is worth noting that these rearrangements require high energies, i.e., energy barriers around 150 kcal·mol^{-1}. Although lower free energy barriers are needed for these transformations at higher temperatures (around 125 kcal·mol^{-1} at 2000 K), it is still difficult and rather unlikely to overcome many of them (see SI for more details). In addition, insertion of a C_2 unit leads to $Sc_2C_2@C_2(43)$-C_{90}, one of the computed lowest energy $Sc_2C_2@C_{90}$ isomers. Therefore, $Sc_2C_2@C_s$(hept)-C_{88} is very likely a *kinetically trapped intermediate*, the most stable among the possible C_{88} nonclassical cages, in a bottom-up growth process from $Sc_2C_2@C_{2v}(9)$-C_{86}.

In order to further test the generality of these findings and to test the validity of the mechanistic interpretations and conclusions, we performed a similar analysis with the first observed EMF containing a heptagon, $LaSc_2N@C_s$(hept)-C_{80}.[11] Remarkably, a simple C_2 insertion of the type depicted in Figure 9a to the non-IPR $LaSc_2N@C_2(22010)$-C_{78}, as shown in Figure 10, leads to the reported heptagon-containing endohedral cage. This non-IPR EMF is at less than 4 kcal mol^{-1} from the lowest energy IPR isomer $LaSc_2N@D_{3h}(5)$-C_{78}, but similar abundances for the two isomers are predicted at $T >$ 2000 K (see SI). The other heptagon-containing fullerene synthesized thus far by the carbon arc process, C_{68}(hept)Cl_6, can also be directly obtained from the $C_{66}(4169)$ precursor

DOI: 10.1021/jacs.6b07912
J. Am. Chem. Soc. 2016, 138, 13030−13037

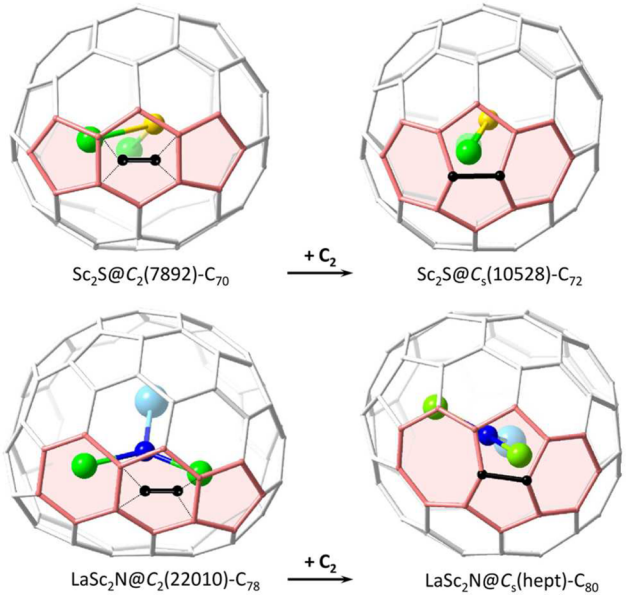

Figure 10. Potential precursors for the observed $LaSc_2N@C_s$(hept)-C_{80} and $Sc_2S@C_s$(10528)-C_{72} EMFs in a bottom-up growth mechanism.

through a C_2 insertion of the type described in Figure 9b,[5] in perfect agreement with a growth mechanism involving a heptagon-containing cage as an intermediate. This was earlier proposed for empty pristine fullerenes in 2001.[40] In addition, very recently, Fowler and co-workers have shown that the preferred nitride EMFs of the C_{78}, C_{80} and C_{82} cages are interconnected by a network of C_2 insertions/extrusions and Stone–Wales isomerization steps in which nonclassical one-heptagon structures may play a significant role.[41] To the best of our knowledge, the only pair of EMFs that can be related by a simple C_2 addition where both have been isolated and characterized so far are $Sc_2S@C_s$(10528)-C_{72}[33] and its potential precursor in a bottom-up growth, $Sc_2S@C_2$(7892)-C_{70}.[42] In contrast to the heptagon-containing EMFs, the C_{70} and C_{72} cages encapsulating a Sc_2S do not exhibit nonclassical heptagon structures at sufficiently low energies. All C_2 insertions of the type shown in Figure 9a on the C_2(7892)-C_{70} tetraanion are above 26 kcal·mol^{-1} relative to the energy of the observed C_s(10528)-C_{72} isomer, which is the optimal C_2 insertion of type b in Figure 9. Table 3 summarizes the computed energies for the lowest energy isomers that can be obtained as a result of C_2 insertions described in Figure 9 (a and b).

To date, the main experimental support for the bottom-up growth mechanism was reported by Kroto and co-workers, who demonstrated that empty and EMFs grow in the presence of a rich carbon vapor atmosphere.[43,44] Here, we report a plausible interpretation compatible with the formation of the two heptagon-containing EMFs known so far, $Sc_2C_2@C_s$(hept)-C_{88} and $LaSc_2N@C_s$(hept)-C_{80}, as well as the classical non-IPR $Sc_2S@C_s$(10528)-C_{72}, from *low energy* precursors and *single* C_2 insertion steps. The main difference between these two nonclassical EMFs is that while $LaSc_2N@C_s$(hept)-C_{80} is highly stabilized by the presence of the cluster, which fits rather well inside this cage, C_s(hept)-C_{88} is already rather stable as a tetraanion. The present interpretation is also in accord with the pioneering theoretical work of Hernández and co-workers,[40] who showed that fullerenes may grow via heptagon intermediates without any Stone–Wales rearrangements. Although extruding C atoms from an already closed fullerene is much more energetically demanding than inserting them in a bottom-up mechanism,[45] it has been found that C_2 extrusion from *nonclassical* carbon cages is favorable at very low carbon-vapor concentrations.[46] This means that the formation of a fullerene, classical or nonclassical, could also follow a *top-down* mechanism,[47] but it is important to mention that to remove a C_2 unit from a classical fullerene, IPR or non-IPR, is not favorable when there is enough carbon vapor concentration in the surrounding atmosphere. We believe that in the following years new evidence will emerge that will help elucidate the formation and growth mechanisms of fullerenes. The carbon cage diversity of EMFs will likely be important to characterize such mechanisms.

Table 3. Relative Energies for the Lowest Energy Anions Obtained as a C_2 Insertion for Several Observed EMFs[a]

EMF	cage precursor	classical fullerene	heptagon fullerene
$Sc_2C_2@C_s$(hept)-C_{88}	C_{2v}(9)-C_{86}	+6.7	0.0
$LaSc_2N@C_s$(hept)-C_{80}	C_2(22010)-C_{78}	+22.3	0.0
$Sc_2S@C_s$(10528)-C_{72}	C_2(7892)-C_{70}	0.0	+26.3

[a]Energies in kcal·mol^{-1} for tetraanions (carbide and sulfide) and hexaanions (nitride).

CONCLUSIONS

In summary, we have successfully synthesized and isolated $Sc_2C_2@C_s$(hept)-C_{88}, which is the first example of an endohedral carbide fullerene with a heptagon ring on the carbon cage and only the second endohedral fullerene to contain a heptagon. The X-ray crystal structure of $Sc_2C_2@C_s$(hept)-C_{88} reveals that a zigzag Sc_2C_2 unit was encapsulated in an unprecedented C_s(hept)-C_{88} cage. Calculations suggest that this endohedral fullerene could be a kinetically trapped species derived from the recently reported $Sc_2C_2@C_{2v}$(9)-C_{86} via a direct C_2 insertion.

EXPERIMENTAL SECTION

Synthesis and Isolation of $Sc_2C_2@C_s$(hept)-C_{88}. A graphite rod was core-drilled, packed with a mixture of Sc_2O_3 and graphite powder (molar ratio of Sc/C = 1:15), and annealed at 1000 °C for 12 h under a nitrogen atmosphere. The graphite rod was then vaporized in a Krätschmer–Huffman-type fullerene generator with an arc current of 82–85 A under 200 mbar helium. The collected soot was Soxhlet-extracted with carbon disulfide for 12 h. The extract was dried using a rotary evaporator. The solid residue was dissolved in toluene and filtered. The desired compound $Sc_2C_2@C_s$(hept)-C_{88} was isolated from empty fullerenes and other endohedral fullerenes by a multiple-stage HPLC process; details are described in the Supporting Information

Spectroscopic Measurements. Vis–NIR spectra were recorded from 400 to 2000 nm in carbon disulfide solution by using a 1.0 cm quartz cell in a Cary 5000 UV–vis–NIR spectrophotometer. MALDI mass spectra were recorded on a Bruker Microflex LRF mass spectrometer. CV experiments were conducted using a CH Instrument Potentiostat. A one-compartment cell with a standard three-electrodes configuration was used, consisting of a 1 mm diameter glassy carbon disk as the working electrode, a platinum wire as counter electrode, and a silver wire as a pseudoreference electrode. A scan rate of 100 mV/s in a solution of *o*-DCB containing 0.05 M *n*-Bu_4NPF_6 was used. Ferrocene was added to the solution at the end of each experiment as an internal potential standard.

Crystal Structure Determination of $Sc_2C_2@C_s$ (hept)-C_{88}·Ni(OEP)·2(C_7H_8). Crystals suitable for X-ray diffraction studies were

DOI: 10.1021/jacs.6b07912
J. Am. Chem. Soc. 2016, 138, 13030–13037

obtained by layering a toluene solution of Ni(OEP) over a toluene solution of $Sc_2C_2@C_s$ (hept)-C_{88} in a 5 mm outside diameter glass tube approximately 18 cm in length.[48] The crystal selected for data collection was a black lath of dimensions 0.020 × 0.028 × 0.075 mm. The crystal was mounted in the 100 K nitrogen cold stream provided by an Oxford Cryostream low temperature apparatus on the goniometer head of a Bruker D8 diffractometer equipped with Bruker Photon 100 CMOS detector. Data were collected with the use of synchrotron radiation (λ = 0.7749 Å) at Beamline 11.3.1 at the Advanced Light Source, Lawrence Berkeley Laboratory. The structure was solved by a dual space method (SHELXT)[49] and refined by full-matrix least-squares on F^2 (SHELXL-2014).[50] The fullerene cage is disordered over two overlapping orientations with statistical (50:50) occupation. By tedious atom picking it was possible to identify two similar cages that each contain a heptagonal ring. The central Sc_2C_2 cluster is likewise disordered. It was possible to find two positions for Sc2, but Sc1 did not clearly split into two positions. The two clusters are therefore modeled as Sc1/C89A/C90A/Sc2A and Sc1/C89B/C90B/Sc2B. The two toluene molecules are disordered over two orientations with relative occupancies 50:50. Some restraints were applied in order to reduce the correlation effects due to overlap. However, all non-hydrogen atoms were refined with anisotropic thermal displacement parameters. Further details of the crystal structure determinations are available in the Supporting Information.

Crystal data: $C_{140}H_{60}N_4NiSc_2$, fw =1946.55, monoclinic, $P2_1/c$, a = 20.834(4) Å, b = 14.965(4) Å, c = 25.689(7) Å, β = 95.603(6)°, V = 7971(3) Å^3, Z = 4, R_1 [20458 reflections with $I > 2\sigma(I)$] = 0.0614, wR_2 (all 25399 unique data) = 0.1771, 2092 parameters, 2217 restraints. Largest diff peak and hole, 1.443 and −3.395 eÅ^{-3}.

Computational Details. We have computed all the tetraanions and hexaanions of C_{88} and C_{90}, respectively, with two or fewer adjacent pentagon pairs (APP) using density functional theory (DFT) methodology with the ADF 2012 program.[51,52] The exchange-correlation functionals of Becke and Perdew (BP86) and the Slater TZP basis sets were employed.[53,54] Dispersion corrections were also included.[55] The lowest energy tetraanionic cages (less than 23 kcal·mol^{-1}) and the lowest energy hexaanionic cages (less than 10 kcal·mol^{-1}) were selected to be calculated in the corresponding endohedral forms. Structures of $Sc_2C_2@C_{88}$ and $Sc_2@C_{90}$ were optimized at the same level of theory. All of the IPR isomers of $Sc_2C_2@C_{86}$ were also computed at the same BP86/TZP level. Car−Parrinello molecular dynamics simulations were carried out using CPMD program.[56,57] The description of the electronic structure was based on the expansion of the valence electronic wave functions into a plane wave basis set, which was limited by an energy cutoff of 90 Ry. The interaction between the valence electrons and the ionic cores was treated through the pseudopotential (PP) approximation (Martins−Troullier type).[58] We included the 3s and 3p semicore electrons in the valence in the Martins−Troullier PP for scandium atoms. The functional by Perdew, Burke, and Ernzerhoff (PBE) was used for the simulations.[59,60] We used a fictitious electron mass of 800 au. The simulations were carried out using periodic boundary conditions in a cubic cell with a side length of 15 Å and a time step of 0.144 fs. See the Supporting Information for more details. Structures and some electronic data for relevant species are available in the Supporting Information and at www.iochem-bd.org/.[61]

■ ASSOCIATED CONTENT

Supporting Information

The Supporting Information is available free of charge on the ACS Publications website at DOI: 10.1021/jacs.6b07912.

Experimental details, HPLC chromatograms of the purified $Sc_2C_2@C_s$(hept)-C_{88}; additional figures and tables with complementary computational results (structural parameters, free energies, molar fractions, etc.) (PDF)

X-ray crystallographic file for $Sc_2C_2@C_s$(hept)-C_{88} (CIF)

■ AUTHOR INFORMATION

Corresponding Authors

*mmolmstead@ucdavis.edu
*albalch@ucdavis.edu
*josepmaria.poblet@urv.cat
*echegoyen@utep.edu

Present Addresses

[‖]Department of Electrochemistry and Conducting Polymers, Leibniz Institute for Solid State and Materials Research, D-01069 Dresden, Germany.
[#]Physical and Life Sciences, Lawrence Livermore National Laboratory, 7000 East Ave., Livermore, California 94550, United States.

Author Contributions

[⊥]C.-H.C. and L.A. contributed equally to the work

Notes

The authors declare no competing financial interest.

Additional supporting research data (structures and some electronic data for relevant species) for this article my be accessed at no charge at http://dx.doi.org/10.19061/iochem-bd-2-7.

■ ACKNOWLEDGMENTS

Dedicated to Prof. Tomas Torres on the occasion of his 65th birthday. L.E. thanks the Robert A. Welch Foundation for an endowed chair and Grant No. AH-0033 and the U.S. NSF (Grant No. CHE-1408865) for generous financial support. A.L.B. and M.M.O. thank the U.S. NSF (Grant No. CHE-1305125) generous financial support. We thank the Advanced Light Source, supported by the Director, Office of Science, Office of Basic Energy Sciences, U.S. Department of Energy under Contract No. DE-AC02-05CH11231 for synchrotron beam time. This work was also supported by the Spanish Ministerio de Ciencia e Innovación (Project No. CTQ2014-52774-P) and the Generalitat de Catalunya (2014SGR-199 and XRQTC). J.M.P. thanks the ICREA foundation for an ICREA ACADEMIA award. L.A. thanks the Generalitat de Catalunya for a predoctoral fellowship (FI-DGR 2014). X.B.P. thanks the Department of Education for a GAANN fellowship.

■ REFERENCES

(1) Kroto, H. W. *Nature* **1987**, *329*, 529.
(2) Yamada, M.; Kurihara, H.; Suzuki, M.; Guo, J. D.; Waelchli, M.; Olmstead, M. M.; Balch, A. L.; Nagase, S.; Maeda, Y.; Hasegawa, T.; Lu, X.; Akasaka, T. *J. Am. Chem. Soc.* **2014**, *136*, 7611.
(3) Schmalz, T. G.; Seitz, W. A.; Klein, D. J.; Hite, G. E. *J. Am. Chem. Soc.* **1988**, *110*, 1113.
(4) Fowler, P. W.; Heine, T.; Mitchell, D.; Orlandi, G.; Schmidt, R.; Seifert, G.; Zerbetto, F. *J. Chem. Soc., Faraday Trans.* **1996**, *92*, 2203.
(5) Tan, Y.-Z.; Chen, R.-T.; Liao, Z.-J.; Li, J.; Zhu, F.; Lu, X.; Xie, S.-Y.; Li, J.; Huang, R.-B.; Zheng, L.-S. *Nat. Commun.* **2011**, *2*, 420.
(6) Troshin, P. A.; Avent, A. G.; Darwish, A. D.; Martsinovich, N.; Abdul-Sada, A. a. K.; Street, J. M.; Taylor, R. *Science* **2005**, *309*, 278.
(7) Ioffe, I. N.; Chen, C.; Yang, S.; Sidorov, L. N.; Kemnitz, E.; Troyanov, S. I. *Angew. Chem., Int. Ed.* **2010**, *49*, 4784.
(8) Ioffe, I. N.; Mazaleva, O. N.; Sidorov, L. N.; Yang, S.; Wei, T.; Kemnitz, E.; Troyanov, S. I. *Inorg. Chem.* **2013**, *52*, 13821.
(9) Yang, S.; Wang, S.; Kemnitz, E.; Troyanov, S. I. *Angew. Chem., Int. Ed.* **2014**, *53*, 2460.
(10) Yang, S.; Wei, T.; Wang, S.; Ioffe, I. N.; Kemnitz, E.; Troyanov, S. I. *Chem. - Asian J.* **2014**, *9*, 3102.
(11) Zhang, Y.; Ghiassi, K. B.; Deng, Q.; Samoylova, N. A.; Olmstead, M. M.; Balch, A. L.; Popov, A. A. *Angew. Chem., Int. Ed.* **2014**, *54*, 495.

DOI: 10.1021/jacs.6b07912
J. Am. Chem. Soc. 2016, 138, 13030−13037

(12) Popov, A. A.; Yang, S.; Dunsch, L. *Chem. Rev.* **2013**, *113*, 5989.
(13) Lu, X.; Feng, L.; Akasaka, T.; Nagase, S. *Chem. Soc. Rev.* **2012**, *41*, 7723.
(14) Wang, T.; Wang, C. *Acc. Chem. Res.* **2014**, *47*, 450.
(15) Lu, X.; Akasaka, T.; Nagase, S. *Acc. Chem. Res.* **2013**, *46*, 1627.
(16) Rodríguez-Fortea, A.; Balch, A. L.; Poblet, J. M. *Chem. Soc. Rev.* **2011**, *40*, 3551.
(17) Yang, S.; Liu, F.; Chen, C.; Jiao, M.; Wei, T. *Chem. Commun.* **2011**, *47*, 11822.
(18) Chaur, M. N.; Melin, F.; Ortiz, A. L.; Echegoyen, L. *Angew. Chem., Int. Ed.* **2009**, *48*, 7514.
(19) Wang, C.-R.; Kai, T.; Tomiyama, T.; Yoshida, T.; Kobayashi, Y.; Nishibori, E.; Takata, M.; Sakata, M.; Shinohara, H. *Angew. Chem., Int. Ed.* **2001**, *40*, 397.
(20) Kurihara, H.; Lu, X.; Iiduka, Y.; Mizorogi, N.; Slanina, Z.; Tsuchiya, T.; Akasaka, T.; Nagase, S. *J. Am. Chem. Soc.* **2011**, *133*, 2382.
(21) Kurihara, H.; Lu, X.; Iiduka, Y.; Nikawa, H.; Hachiya, M.; Mizorogi, N.; Slanina, Z.; Tsuchiya, T.; Nagase, S.; Akasaka, T. *Inorg. Chem.* **2012**, *51*, 746.
(22) Iiduka, Y.; Wakahara, T.; Nakajima, K.; Nakahodo, T.; Tsuchiya, T.; Maeda, Y.; Akasaka, T.; Yoza, K.; Liu, M. T. H.; Mizorogi, N.; Nagase, S. *Angew. Chem., Int. Ed.* **2007**, *46*, 5562.
(23) Chen, C.-H.; Yeh, W.-Y.; Liu, Y.-H.; Lee, G.-H. *Angew. Chem., Int. Ed.* **2012**, *51*, 13046.
(24) Zhang, J.; Bowles, F. L.; Bearden, D. W.; Ray, W. K.; Fuhrer, T.; Ye, Y.; Dixon, C.; Harich, K.; Helm, R. F.; Olmstead, M. M.; Balch, A. L.; Dorn, H. C. *Nat. Chem.* **2013**, *5*, 880.
(25) Yang, H.; Lu, C.; Liu, Z.; Jin, H.; Che, Y.; Olmstead, M. M.; Balch, A. L. *J. Am. Chem. Soc.* **2008**, *130*, 17296.
(26) Sado, Y.; Aoyagi, S.; Izumi, N.; Kitaura, R.; Kowalczyk, T.; Wang, J.; Irle, S.; Nishibori, E.; Sugimoto, K.; Shinohara, H. *Chem. Phys. Lett.* **2014**, *600*, 38.
(27) Liu, F.; Wei, T.; Wang, S.; Guan, J.; Lu, X.; Yang, S. *Fullerenes, Nanotubes, Carbon Nanostruct.* **2014**, *22*, 215.
(28) Chen, C.-H.; Ghiassi, K. B.; Cerón, M. R.; Guerrero-Ayala, M. A.; Echegoyen, L.; Olmstead, M. M.; Balch, A. L. *J. Am. Chem. Soc.* **2015**, *137*, 10116.
(29) Cai, W.; Bao, L.; Zhao, S.; Xie, Y.; Akasaka, T.; Lu, X. *J. Am. Chem. Soc.* **2015**, *137*, 10292.
(30) Cai, W.; Li, F.-F.; Bao, L.; Xie, Y.; Lu, X. *J. Am. Chem. Soc.* **2016**, *138*, 6670.
(31) Zhang, J.; Fuhrer, T.; Fu, W.; Ge, J.; Bearden, D. W.; Dallas, J.; Duchamp, J.; Walker, K.; Champion, H.; Azurmendi, H.; Harich, K.; Dorn, H. C. *J. Am. Chem. Soc.* **2012**, *134*, 8487.
(32) Deng, Q.; Popov, A. A. *J. Am. Chem. Soc.* **2014**, *136*, 4257.
(33) Chen, N.; Beavers, C. M.; Mulet-Gas, M.; Rodríguez-Fortea, A.; Munoz, E. J.; Li, Y.-Y.; Olmstead, M. M.; Balch, A. L.; Poblet, J. M.; Echegoyen, L. *J. Am. Chem. Soc.* **2012**, *134*, 7851.
(34) Shinohara, H. *Rep. Prog. Phys.* **2000**, *63*, 843.
(35) Yang, H.; Jin, H.; Zhen, H.; Wang, Z.; Liu, Z.; Beavers, C. M.; Mercado, B. Q.; Olmstead, M. M.; Balch, A. L. *J. Am. Chem. Soc.* **2011**, *133*, 6299.
(36) Yang, H.; Jin, H.; Hong, B.; Liu, Z.; Beavers, C. M.; Zhen, H.; Wang, Z.; Mercado, B. Q.; Olmstead, M. M.; Balch, A. L. *J. Am. Chem. Soc.* **2011**, *133*, 16911.
(37) Zuo, T.; Beavers, C. M.; Duchamp, J. C.; Campbell, A.; Dorn, H. C.; Olmstead, M. M.; Balch, A. L. *J. Am. Chem. Soc.* **2007**, *129*, 2035.
(38) Slanina, Z.; Lee, S.-L.; Uhlík, F.; Adamowicz, L.; Nagase, S. *Theor. Chem. Acc.* **2007**, *117*, 315.
(39) Slanina, Z.; Nagase, S. *ChemPhysChem* **2005**, *6*, 2060.
(40) Hernández, E.; Ordejón, P.; Terrones, H. *Phys. Rev. B: Condens. Matter Mater. Phys.* **2001**, *63*, 193403.
(41) Gan, L.-H.; Lei, D.; Fowler, P. W. *J. Comput. Chem.* **2016**, *37*, 1907.
(42) Chen, N.; Mulet-Gas, M.; Li, Y.-Y.; Stene, R. E.; Atherton, C. W.; Rodríguez-Fortea, A.; Poblet, J. M.; Echegoyen, L. *Chem. Sci.* **2013**, *4*, 180.
(43) Dunk, P. W.; Kaiser, N. K.; Hendrickson, C. L.; Quinn, J. P.; Ewels, C. P.; Nakanishi, Y.; Sasaki, Y.; Shinohara, H.; Marshall, A. G.; Kroto, H. W. *Nat. Commun.* **2012**, *3*, 855.
(44) Dunk, P. W.; Mulet-Gas, M.; Nakanishi, Y.; Kaiser, N. K.; Rodríguez-Fortea, A.; Shinohara, H.; Poblet, J. M.; Marshall, A. G.; Kroto, H. W. *Nat. Commun.* **2014**, *5*, 5844.
(45) Mulet-Gas, M.; Abella, L.; Dunk, P. W.; Rodríguez-Fortea, A.; Kroto, H. W.; Poblet, J. M. *Chem. Sci.* **2015**, *6*, 675.
(46) Saha, B.; Irle, S.; Morokuma, K. *J. Phys. Chem. C* **2011**, *115*, 22707.
(47) Zhang, J.; Bowles, F. L.; Bearden, D. W.; Ray, W. K.; Fuhrer, T.; Ye, Y.; Dixon, C.; Harich, K.; Helm, R. F.; Olmstead, M. M.; Balch, A. L.; Dorn, H. C. *Nat. Chem.* **2013**, *5*, 880.
(48) Olmstead, M. M.; Costa, D. A.; Maitra, K.; Noll, B. C.; Phillips, S. L.; Van Calcar, P. M.; Balch, A. L. *J. Am. Chem. Soc.* **1999**, *121*, 7090.
(49) Sheldrick, G. *Acta Crystallogr., Sect. A: Found. Adv.* **2015**, *71*, 3.
(50) Sheldrick, G. *Acta Crystallogr., Sect. C: Struct. Chem.* **2015**, *71*, 3.
(51) te Velde, G.; Bickelhaupt, F. M.; Baerends, E. J.; Fonseca Guerra, C.; van Gisbergen, S. J. A.; Snijders, J. G.; Ziegler, T. *J. Comput. Chem.* **2001**, *22*, 931.
(52) Baerends, E. J.; Ellis, D. E.; Ros, P. *ADF 2012.01*; Department of Theoretical Chemistry, Vrije Universiteit: Amsterdam, 2012.
(53) Becke, A. D. *Phys. Rev. A: At., Mol., Opt. Phys.* **1988**, *38*, 3098.
(54) Perdew, J. P. *Phys. Rev. B: Condens. Matter Mater. Phys.* **1986**, *33*, 8822.
(55) Grimme, S.; Ehrlich, S.; Goerigk, L. *J. Comput. Chem.* **2011**, *32*, 1456.
(56) *CPMD*. http://www.cpmd.org. Copyright IBM Corp. 1990−2015, Copyright MPI für Festkörperforschung Stuttgart 1997−2001.
(57) Car, R.; Parrinello, M. *Phys. Rev. Lett.* **1985**, *55*, 2471.
(58) Troullier, N.; Martins, J. L. *Phys. Rev. B: Condens. Matter Mater. Phys.* **1991**, *43*, 1993.
(59) Perdew, J. P.; Burke, K.; Ernzerhof, M. *Phys. Rev. Lett.* **1996**, *77*, 3865.
(60) Perdew, J. P.; Burke, K.; Ernzerhof, M. *Phys. Rev. Lett.* **1997**, *78*, 1396.
(61) Álvarez-Moreno, M.; De Graaf, C.; Lopez, N.; Maseras, F.; Poblet, J. M.; Bo, C. *J. Chem. Inf. Model.* **2015**, *55*, 95−103.

DOI: 10.1021/jacs.6b07912
J. Am. Chem. Soc. 2016, 138, 13030−13037